Space Sci Rev (2008) 141: 185–211
DOI 10.1007/s11214-008-9386-4

Instrument Boom Mechanisms on the THEMIS Satellites; Magnetometer, Radial Wire, and Axial Booms

David Auslander · Joshua Cermenska · Gregory Dalton · Mauricio de la Pena · C.K.H. Dharan · William Donokowski · Robert Duck · Jonghak Kim · David Pankow · Alec Plauche · Mustapha Rahmani · Stephen Sulack · Tien Fak Tan · Paul Turin · Tyler Williams

Received: 24 April 2008 / Accepted: 21 May 2008 / Published online: 17 June 2008

Abstract The five "Time History of Events and Macroscale Interactions during Substorms" (THEMIS) micro-satellites launched on a common carrier by a Delta II, 7925 heavy, on February 17, 2007. This is the fifth launch in the NASA MeDIum class EXplorer (MIDEX) program. In the mission proposal the decision was made to have the University of California Berkeley Space Sciences Laboratory (UCB-SSL) mechanical engineering staff provide all of the spacecraft appendages, in order to meet the short development schedule, and to insure compatibility. This paper describes the systems engineering, design, development, testing, and on-orbit deployment of these boom systems that include: the 1 and 2 meter carbon fiber composite magnetometer booms, the 40 and 50 m tip to tip orthogonal spin-plane wire boom pairs, and the 6.3 m dipole stiff axial booms.

Keywords THEMIS · Magnetosphere · Radiation belts · Magnetopause · Constellation · Mechanisms

PACS 94.30.-d · 94.30.cl · 94.30.cb · 94.30.ch · 94.30.cj · 94.30.C- · 94.30.cp · 94.30.Lr · 94.30.Va · 94.30.Xy · 96.50.Fm

1 Introduction

1.1 Mission Background

The scientific objectives of this magnetospheric physics mission are to investigate many of the fundamental questions on the nature of magnetic sub-storm instabilities. The spatial nature of these activities dictates the need for multiple synchronized probes (Angelopoulos

D. Auslander · J. Cermenska · M. de la Pena · C.K.H. Dharan · J. Kim · M. Rahmani · S. Sulack · T.F. Tan · T. Williams
Mechanical Engineering Department, University of California, Berkeley, USA

G. Dalton · W. Donokowski · R. Duck · D. Pankow (✉) · A. Plauche · P. Turin
Samuel Silver Space Sciences Laboratory, University of California, Berkeley, USA
e-mail: dpankow@ssl.berkeley.edu

2008). Each of the five identical probes has a complete science package. Probes are coordinated by our ground based missions operations center.

The Electric Fields Instrument (EFI), Electrostatic Analyzer (ESA), and Solid State Telescopes (SST) were all provided by the University of California Berkeley (UCB). The Fluxgate Magnetometer (FGM) was provided by the Technical University of Braunschweig, (TU-BS), Germany. The Search Coil Magnetometer (SCM) was provided by Centre des Environements Terrestre et Planétaires (CETP), France. The two Magnetometer Booms were provided by UCB. The Instrument Data Processing Unit was provided by UCB. The Probe Carrier and five Probe Buses with avionics were provided by Swales Aerospace under contract to UCB. Delta II launch services were provided by United Launch Alliance under contract to NASA Kennedy Space Flight Center Dr. Vassilis Angelopoulos of UCB was the mission Principal Investigator. Peter Harvey was the UCB Project Manager. Frank Snow was the GSFC Explorers Office Mission Manager.

1.2 Spacecraft Boom Sensors Configuration

Three orthogonal dipoles with six tip mounted sensors are needed for a vector measurement of the DC and AC electric fields in the plasma. Sounding rocket and early satellite experiments used stiff, deployable booms for the dipoles. Solar-thermal bending and vehicle dynamics severely limited these stiff booms to lengths of several meters, far short of the lengths desired for more precise physical measurements. In the evolution of these instruments, the preferred practical configuration has been found to be a spinning vehicle with four limp wires in the "spin plane" and two stiff axial booms along the spin axis. The limp wires can be precisely positioned by centripetal acceleration, and are immune to the bending and buckling concerns in stiff booms. These lightweight wires allowed about a tenfold increase in the practical radial boom dipole lengths. The SCM and FGM are mounted on stiff CFRP booms for immunity to bus induced and stray fields, as well as one another. The particle instruments, ESA and SST's are probe mounted with outward looking, clear fields of view.

1.3 Spacecraft Stability Constraints

In practice, boom lengths are determined by the need for a spin stable vehicle. Briefly stated, a spinning body will be passively stable about the principal axis having the largest principal moment of inertia, based on conservation of angular momentum and body-flexing dissipation of energy to a rotational energy minimum (Meirovitch and Calico 1972). The spin stability ratio (which must be >1) is defined as the ratio of the moment of inertia about the spin axis to the larger of the two transverse axes ($I_s/I_{T\max}$), while the stability margin is defined as this ratio minus one. This means the radial wire booms improve stability and can be quite long, while the axial booms are length limited because they reduce the stability margin by increasing the transverse moment of inertia. The wire boom cables are essentially limp to any transient motions or oscillations induced by spacecraft maneuvers. The resulting pendulum behavior is mostly dependent on the wire root or hinge attachment radius, the distance from the spin axis to the wire attachment, or exit point. The deployed wire boom plane was located close to the spacecraft Z axis center of mass to avoid spin axis tilt caused by wire boom mass moment asymmetries. The axial booms must be sufficiently rigid to avoid elastic instability and subsequent collapse. As previously stated, the vehicle stability margin severely limits the axial boom length. In the mission planning stages, it was decided to include the stabilizing effect of wire booms in the overall moment of inertia calculations, to maximize the allowed axial boom length. In practice this increased the

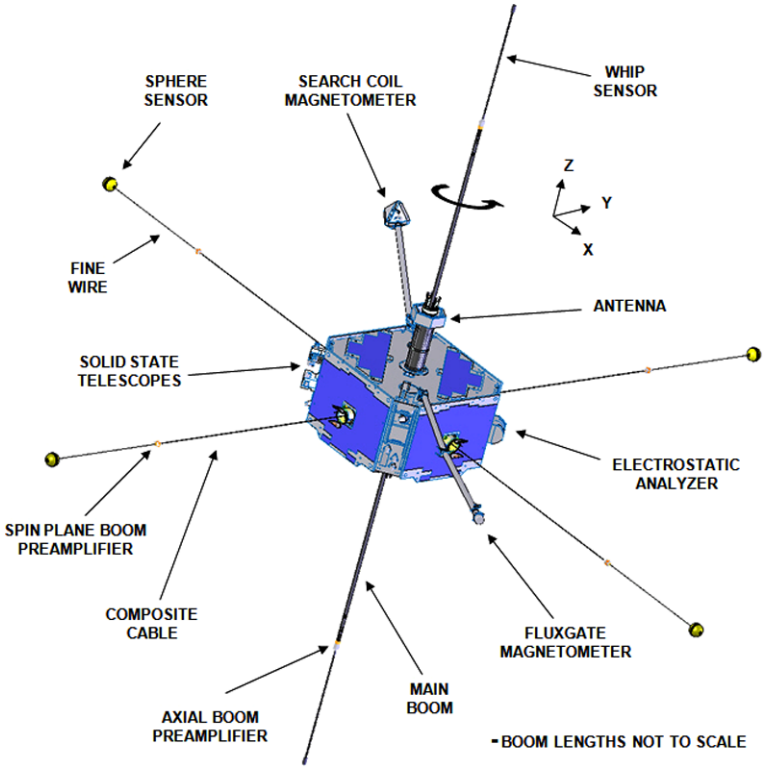

Fig. 1 On orbit deployed booms configuration

boom length from 2.6 m to 3.2 m each, which is a very significant improvement for minimizing the effects of vehicle photo-electron emission. Conventional wisdom suggests that boom length might be increased by decreasing the boom mass, which will also decrease the stiffness. However, spin induced boom flexing amplifies the 'effective' boom second mass moment (Meirovitch and Calico 1972). A boom cantilever resonance of four times the spin (as compared to a customary requirement of two) was selected to maximize boom length. A systems level concern was evaluation of the spin axis alignment budget. A list of many uncertainties, ranging from deployed boom straightness to alignment of the vehicle balance fixtures, will affect the alignment of the spin axis with the vehicle geometric axis. Simple addition of this list is far too conservative, and not warranted. If each of the uncertainties is assumed to have random clocking with respect to the spin axis, the resulting imbalance is half the root square summation (RSS) of these residual inertia products. The traditional NASA minimum requirement for the vehicle stability margin is 4%, based mostly in the uncertainties of mass moment measurements. Sensitivity of the spin axis alignment indicated that a more practical stability minimum was 8–10% for most satellites. The probe stability margins range from 16 to 25%, a function of the remaining fuel.

The on orbit deployment sequence serially released the magnetometer booms, the radial wire booms, then the axial booms. For both enhanced reliability and simplicity, these boom mechanisms are purposely designed without a retraction capability. The boom systems were manually rewound and reset after ground testing, and on orbit retraction is neither possible nor necessary.

1.4 Spacecraft Dynamic Simulations

A central feature of the Themis mission is the synchronized one, two and four day probe orbits, which were predicted to include very significant station keeping maneuvers. Each probe has only four thrusters; tangential spin and despin thrusters plus two axial thrusters pointed in the $-Z$ direction. Each of these pairs is diametrically opposed so that they may also be used in pairs. The two axial thrusters are needed for the timely and very large velocity change maneuvers needed to initially place the probes in the desired orbits. The flexible booms are not yet deployed during these early maneuvers. Many of the later maneuvers were known to be most effective at perigee, which would call for both timely and aggressive action. The probe science attitude has its spin vector close to orbit normal. The fuel needed to tip the spin axis into the orbit plane with all booms deployed is prohibitive, which meant that most of the later orbit delta velocity maneuvers would need to be performed by synchronous pulsing of the tangential and opposite spin and despin thrusters. The second vital maneuver was spin axis pointing to maintain the desired probe science attitude, which would be achieved by pulsing of one of the radial offset spin axis thrusters. In the context of probe dynamic time constants, it was expected that these two pulsed maneuvers would reach steady state, the equivalent of pulsing forever in the simulations. At launch, the probe mass was 40% fuel in two non-restrictive spherical tanks, which meant that pulse excited fuel slosh would be a major maneuvering constraint. Short pulses could reduce slosh, but are also known to reduce thruster specific impulse. One goal of these studies was to maximize pulse widths, consistent with attitude stability.

Given the critical nature of these maneuvers, two teams of graduate students developed independent parallel simulations, guided by David Auslander. One team developed simulations in Matlab-Simmechanics while the other worked in a "home brew" C++ environment. The initial ground rules were that observed modal frequencies needed to agree to a few percent and amplitudes to perhaps 25%. These simulations were both developed using techniques pioneered by Auslander (2000), where the desired multi-body dynamics were developed using only a small manifold of point masses connected by springs. Distributed mass rigid bodies were represented by six, or more, point masses inter-connected with very stiff springs. A third independent confirmation of the simulation results was also developed by David Pankow, using the published analytic results of Lai and Bhavnani (1975). Figure 2 provides the various oscillation modes. The slosh modes are similar, but with only two tanks.

In the early stages of simulations development, sub-models confirmed that the limp radial booms could be adequately represented by a simple point mass 3D pendulum with all of the actual hardware mass positioned at the computed Center of Percussion about the wire exit, or hinge point. Similar sub-models confirmed that each stiff axial boom could be represented by an ensemble of 24 properly chosen springs and 12 point masses. Published slosh damping characteristics by Franklin Dodge (2000), which is an update of NASA-SP106, were used to model the fuel mass behavior as a slug mass 3D pendulum. The spherical tank geometry dictates the pendulum length as a function of fuel fill. Both the radial wire booms and the fuel pendulums are inherently limp, which meant the apparent pendulum stiffness is provided by the probe spin forces. One dynamic simulation rule of thumb is that appendages with a first resonant mode greater than four times the spin may be considered to be rigid, with modest loss of fidelity. With this, the >3 Hz magnetometer booms were assumed rigid, lumping their mass moments into the probe hub.

The analytic and numeric results identified semi-resonant slosh conditions where the fuel pendulum slosh period is some integer multiple of the spin period. With continuous pulsed thrusting this causes the familiar, and troublesome, resonant amplification. The smooth,

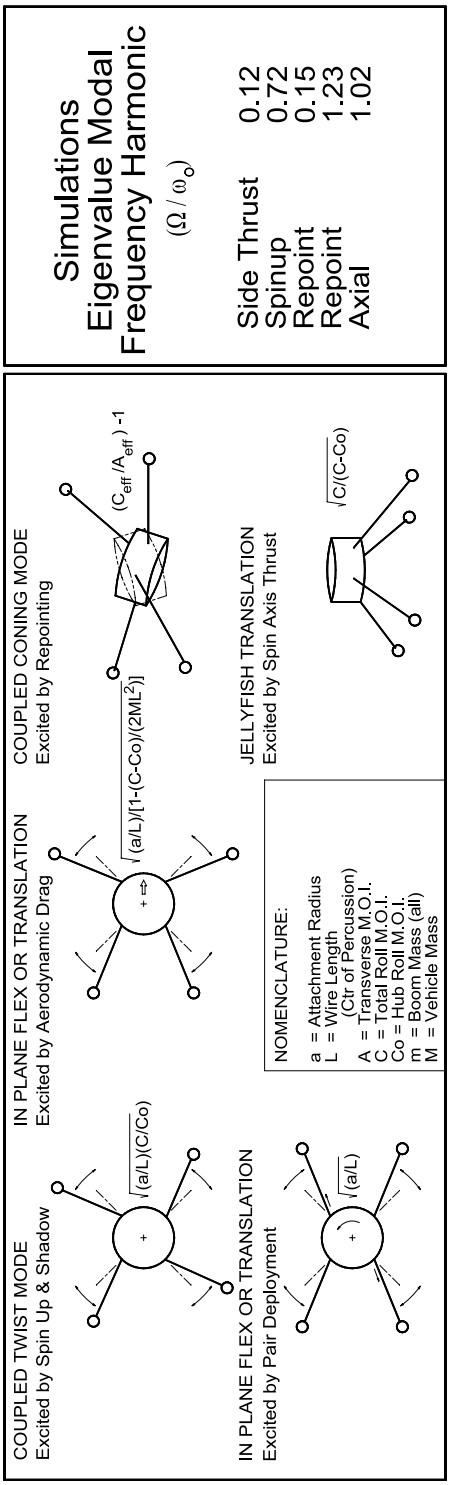

Fig. 2 Rotation and translation modes of a central hub with four wire booms

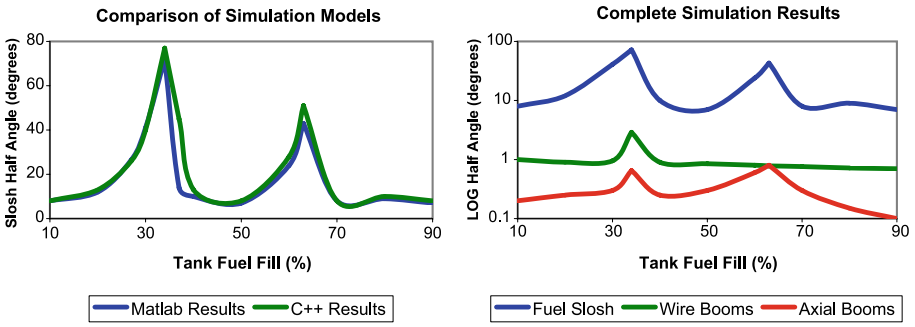

Fig. 3 Synchronous pulsed (±30°/360°) side thrusting results

spherical tanks provide very little laminar flow, viscid damping. Stated in familiar engineering terms, for a single degree of freedom system, the maximum native Q (resonant amplification) is 350 at 50% fill. For side thrusting these harmonics were at 34 and 63% fuel fill. For pointing maneuvers these harmonics are at 20 and 60% fuel fill. These are different because of the physical nature of the spin induced centripetal acceleration. In side thrusting the fuel moves in the spin plane and the centripetal acceleration vector must point radially inward to the spin center. In pointing maneuvers, the fuel moves out of the spin plane and centripetal acceleration vector must be orthogonal to the spin vector. The radial wire booms do not experience these near resonant conditions. Given the limp pendulum representations of both fuel and wires, the ratio of pendulum periods to spin period is dictated by physical geometry only. This means that probe spin rate changes cannot be used to avoid the near resonant conditions.

Figure 3 presents side thrusting results from the complete simulation models as a function of fuel fill. The left plot provides a comparison of the two independent models. The amplitudes are peak values from the models response, where the multi-mode oscillations typically showed beating patterns, as later illustrated in Fig. 4. The right plot compares the response of all probe flexible elements. The modest response peaks reflect only weak coupling of flexible elements, given adequate separation of resonant conditions. The simultaneous peaks reflect a larger hub motion, which may be viewed as a larger base input for all elements, rather than element to element coupling. The ±30 pulse width was felt to be an upper bound for maintaining high specific impulse, given the directional variations during each pulse. Hence, added investigation of pulse widths was not pursued.

Figure 4 presents the pointing maneuver model results, where the limiting factor was slosh amplitude, which is presented as a function of fuel fill. The right plot illustrates the beating behavior which was typical in all results. This plot also illustrates the modest settling time constant, which was needed for mission maneuver planning.

Figure 5 presents the pointing maneuver probe nutation and slosh model results at 20 and 40% fuel fill. These typical preliminary results were used to select a baseline 12° half pulse width for the later detailed simulations.

The full simulation results were reviewed with the Themis Mission Operations Team and used as the basis for the Maneuvering Flight Rules. Nominal pulse widths of ±30° for side thrusting and ±12° for pointing were selected. The side thrust pulse would be reduced to ±20° when the fuel is 29–39% or 58–68% to moderate the response peaks. The ±12° pointing pulse behavior was judged to be adequate at all tank levels. One additional maneuver that is sometimes used is the so called “beta thrusting” where radial and axial thrusters are

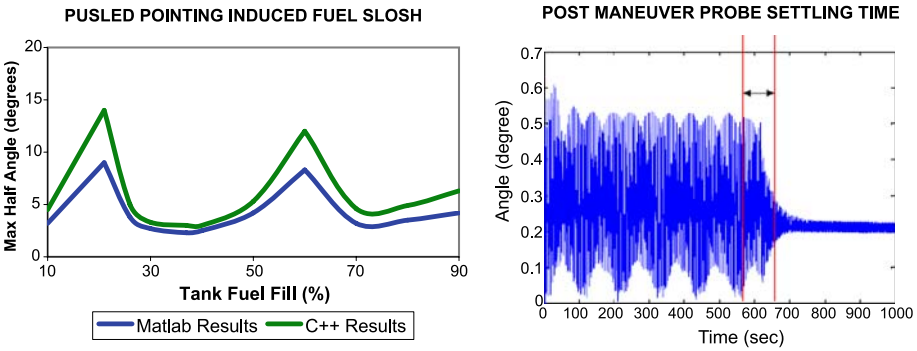

Fig. 4 Pointing induced slosh and post maneuver nutation settling results

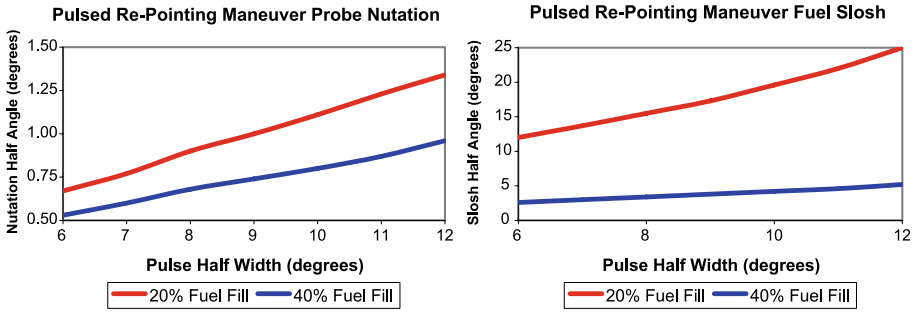

Fig. 5 Pointing induced nutation and fuel slosh as a function of pulse width

simultaneously pulsed to provide a velocity change at the angle beta to the spin plane. The simulations indicated smaller pulse widths would be needed, and small time saving as compared to sequential axial and radial thrusting. Beta thrusting was not included in the flight rules.

2 The Magnetometer Boom Mechanisms

2.1 Magnetometer Boom Science Configuration

The magnetometer booms are stowed during launch and deployed to provide rigid support for accurate pointing of the magnetometers while keeping the magnetometers far enough away from the main body of the satellite to avoid the magnetic interference from small current loops in the onboard circuitry. Each probe has two magnetometer booms. One supports the Flux Gate Magnetometer (FGM) approximately 2-m away from the probe. The other supports the Search Coil Magnetometer (SCM) approximately 1-m away from the probe. A picture of the deployed magnetometer booms is shown in Fig. 6.

The design of the magnetometer booms takes into account a variety of mission requirements. The magnetometer booms must fit on the top deck of the probe. Additionally, the probe and carrier must fit in the Delta II launch fairing. The masses of the FGM magnetometer boom (FGB) and SCM magnetometer boom (SCB) and instrument are also limited.

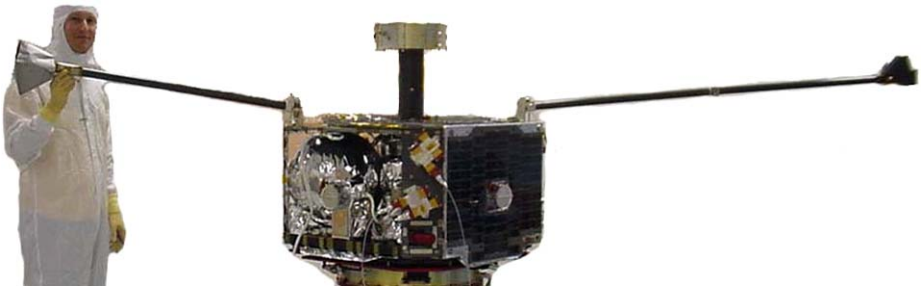

Fig. 6 Deployed magnetometer booms; SCB on *left* and FGB on *right*

In the deployed configuration, the largest of the three principal moments of inertia must line up with probe spin axis within 1 degree. The magnetometer boom deployment shall be repeatable to 1 degree with stability better than 0.1 degrees.

The magnetometer booms must survive the vibration loading from launch and the stresses from deployment between 2 to 18 RPM. Additionally, since the booms are mounted outside the probe, they must survive thermal cycling between 75°C to −115°C. The magnetometer booms must also meet magnetic cleanliness of less than 0.1 nT and carry the harnessing from the magnetometers to the probe.

2.2 Magnetometer Boom Design

To meet the accuracy and repeatability requirements, a rigid unfolding link design is used with one link for the SCB and two links for the FGB. The spinning dynamics of the deployment and packaging constraints dictated that the booms would be located on the upper deck of the spacecraft, unfolding along axes parallel to the spacecraft spin axis. This configuration is shown in Fig. 7.

The SCB consists of a composite boom segment with the base hinge assembly and magnetometer on opposite ends. When the SCB is stowed, it is clamped via a frangible Ti bolt (Frangibolt) to a (Deployment Assist Device) DAD tower that contains the shape memory alloy (SMA) deployment device (TiNi Aerospace, San Leandro, CA), and the Search Coil Magnetometer instrument and interface.

The FGB consists of two composite boom segments. The inner segment is attached to the base hinge and the outer segment is attached to the magnetometer. The two segments are attached together with an elbow hinge. When the FGB is stowed, the two boom segments are folded parallel and held near the base spring with a SMA deployment device. The elbow hinge is held in a bracket with disc springs to help keep the stowed boom latched and aid deployment.

Generally, the magnetometer boom's fittings and deployment mechanisms are machined out of non-magnetic metals like aluminum, bronze and beryllium copper. However, the use of composite booms instead of metallic booms is advantageous in the design of the magnetometer booms. The booms are stowed as 1 m lengths during launch to minimize the mass due to clamping and the necessary release mechanisms. The high specific stiffness of composites easily met the frequency requirements. Additionally, the composite boom is designed to have minimal thermal expansion to match that of the composite deck when exposed to on orbit temperature extremes. The composite tubes are also nonmagnetic and their low density minimizes the mass budget of the magnetometer booms.

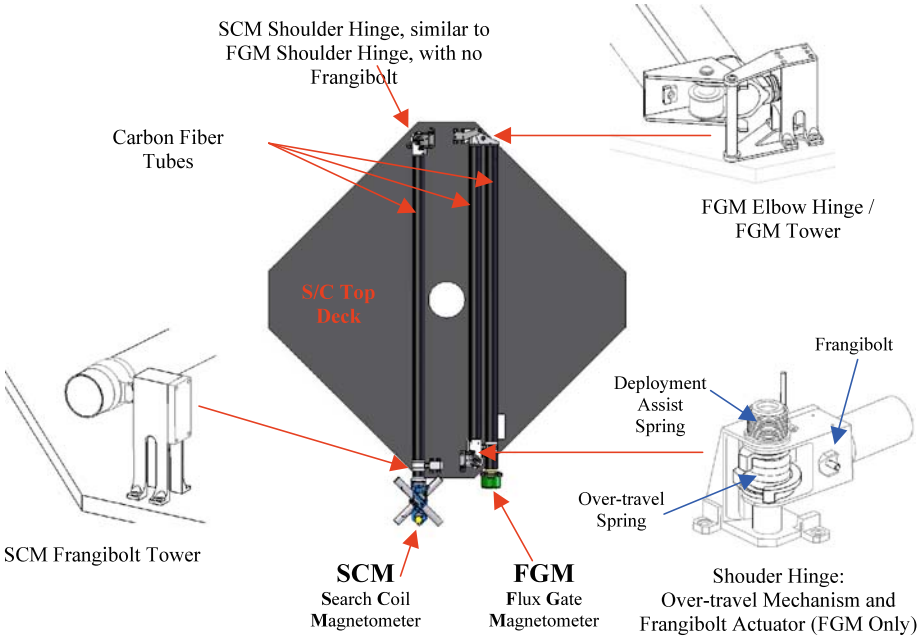

Fig. 7 Magnetometer boom configuration

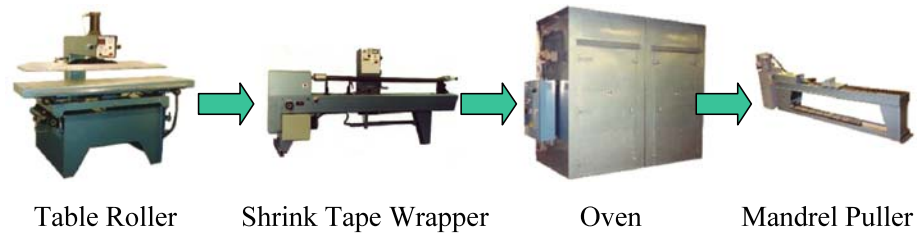

Fig. 8 Magnetometer boom CFRP tube fabrication

Carbon fiber/RS-3 prepreg were used to fabricate the magnetometer boom tubes. The booms are designed using quasi-isotropic high strength T300 carbon fiber fabric to provide shear, hoop and handling strength and ultra high modulus M55J unidirectional carbon fiber to provide longitudinal stiffness. The layup is also designed to minimize coefficient of thermal expansion. The RS-3 (YLA, Benicia, CA) cyanate ester matrix with a 170°C cure temperature was selected, to ensure low outgassing and dimensional stability of the composites.

The composite booms are fabricated by Berkeley Composites Laboratory using the tube rolling process (Century Design, San Diego, USA). The tube rolling process uses a tube roller, shrink tape wrapper, cure oven and mandrel extractor, as shown in Fig. 8. The prepreg is rolled around a hard anodized aluminum mandrel coated with a release agent using the table roller with controlled rolling speed, pressure, and lower platen heat. The mandrel with the prepreg rolled around it is then transported onto the shrink tape wrapper machine where tape is wrapped around the tube with constant tension and speed control. A convection

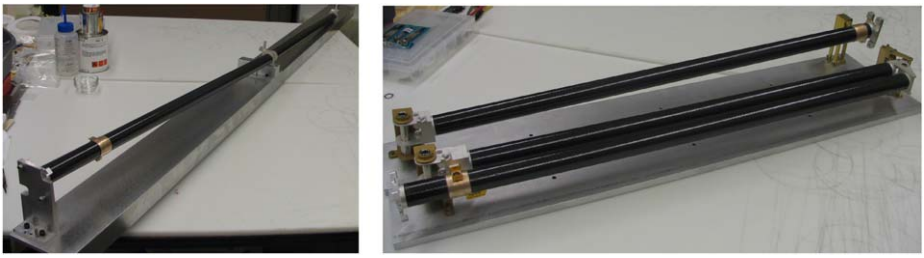

Fig. 9 Magnetometer boom in bonding fixtures

oven is used to cure the booms at 170°C for two hours. Once the booms are cooled to room temperature, a chain driven mandrel extractor is used to extract the boom from the aluminum mandrel. This process provided consistent through thickness consolidation of the composites and the minimized part to part variability.

The composite booms are then finished by high speed machining before integrating with the deployment mechanisms. Special bonding fixtures, shown in Fig. 9, are designed with tight flatness tolerances to first bond the composite booms to the end fittings in the deployed position (with a longitudinal cant and axial twist) to ensure boom accuracy. Hysol EA 9394 (Henkel, Düsseldorf, Germany) is used as the bonding adhesive to ensure high temperature stability. The composite boom tubes are bonded on the inside surfaces to aluminum fittings.

The next step is to bond the saddle rings onto the composite booms in their stowed configuration. The FGB is folded and stowed using the Frangibolt simulator, and saddle ring is bonded to the outside of the composite boom tube. Similarly, the SCB saddle ring is stowed using the clamping mechanism and bonded to the outside of the composite boom tube.

2.3 Magnetometer Boom Deployment Mechanisms

The base hinge assembly in both booms contains three custom beryllium copper springs: the deployment spring, latch pin spring and saloon door spring. During deployment, the deployment torsion spring assists centripetal forces and acts on the booms as they deploy and latch. The latch is engaged when a spring-loaded bronze pin with PTFE impregnated Acetal tip insert springs into a gap between two rotating cogs. At this point, the saloon door spring engages. After the kinetic energy is dissipated, the deployment spring holds the boom against the hard stop of these preloaded cogs. The base hinge assembly is constructed of aluminum, to save weight, and has kinematic flexure mounting points to minimize thermal stresses between the carbon fiber deck and aluminum bracket and to provide stable pointing through thermal cycles.

The magnetometer booms are deployed when the spacecraft is in orbit and spinning, in the following sequence: 1) the SMA deployment device are activated, breaking the Frangibolts which secure the booms during launch; 2) the SCB and outer segment of the FGB begin to open; 3) at approximately 20° of deployment, the elbow latch releases, freeing the inner segment of the FGB to begin deploying; 4) as the outer segment of the FGB opens along with the inner link of the FGB, it is slowed by coriolis acceleration; 5) when the booms deploy to their final position, the "saloon door" style hinges engage, and excess energy is lost in the ensuing oscillations while the booms settle to their final positions which are positively defined by the saloon door springs. The sequence is shown in Fig. 10. Detailed Matlab simulations confirmed the deployment dynamics, torque margins, and peak loads.

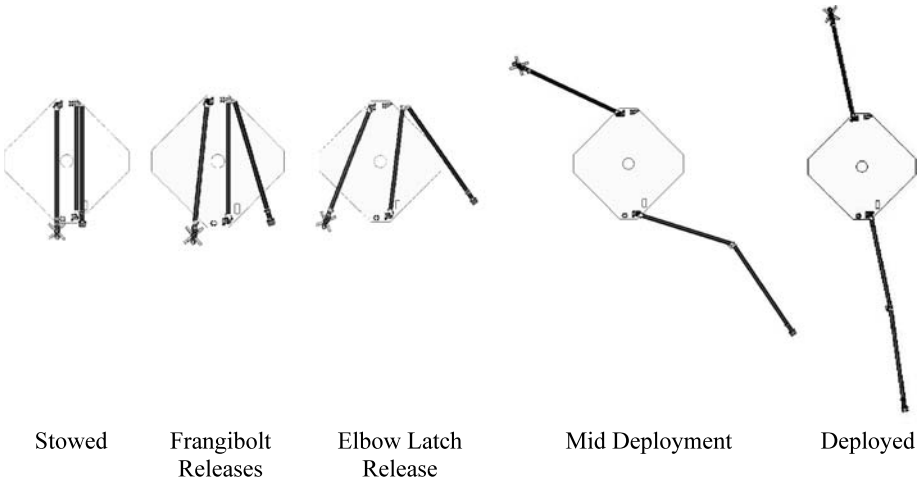

Fig. 10 Magnetometer boom deployment sequence

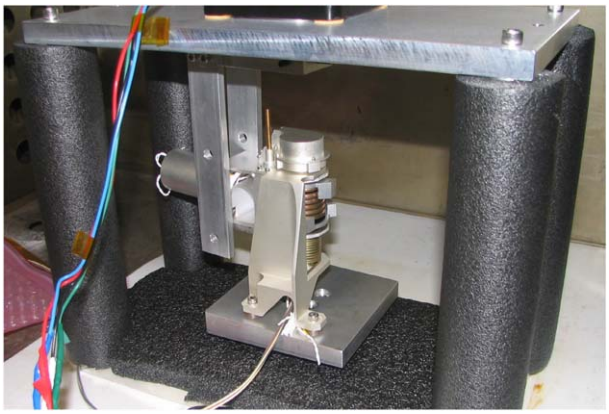

Fig. 11 Torque margin test fixture

2.4 Magnetometer Boom Testing

Before assembly of multiple flight units, proof testing is performed on the various components of the design. The composite booms are designed by theoretical and numerical analyses and optimized by testing on the vibration table. A key concern of the composite boom is their bonding with aluminum end and the potential large thermal mismatch. The bonding interface design and technique is proven by thermally cycling a short composite boom bonded to an aluminum end fitting.

The deployment hinge mechanisms are tested for fit by constructing rapid prototyping parts. After the flight hinge mechanism is fabricated, a torque margin test of the hinge is conducted at the deployment temperature extremes. The torque margin test fixture, shown in Fig. 11, consists of a stepper motor, which rotates the free end and a load cell which measured the torque at the fixed end. The difference in torque levels measured in stowing and deployment motions are used to determine the torque margin.

After assembling the magnetometer boom, each magnetometer boom is statically proof tested with the quasi-static equivalent load along each axis. This static test loads the mount-

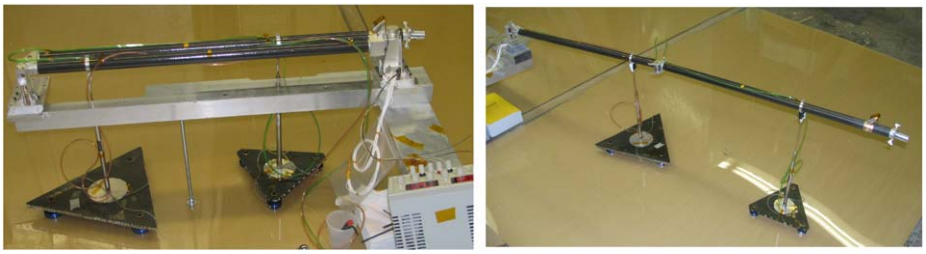

Fig. 12 Stowed (*left*) and Deployed (*right*) FGB

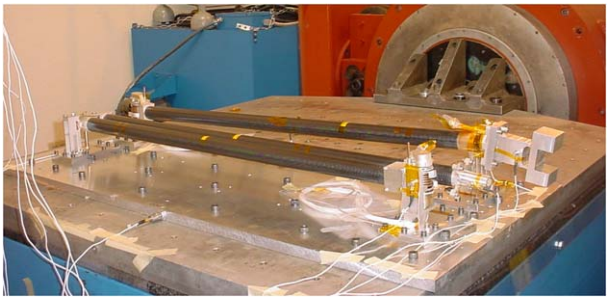

Fig. 13 Vibration test of magnetometer booms

ing points, clamping Frangibolts, the composite boom and the composite/aluminum interface.

Next, the deployment of the stowed magnetometer boom is functionally tested by performing a conservative 0 RPM deployment test. The friction from moment due to magnetometer boom weight and the magnetometer boom tilting up when the boom rotates complicates the deployment test. To eliminate these two problems, air pistons are use to offset the magnetometer boom's weight. The air piston's force is controlled by pressure and the constant force of air pistons as they extend allow for continuous weight offset of the magnetometer booms as they tilt up when deploying. The air pistons are mounted on a low-mass composite sandwich panel, fitted with low friction air bearings and allowed to travel along on a smooth, acrylic base as the magnetometer boom deploys. The stowed and deployed FGB with weight offset devices are shown in Fig. 12.

After deployment testing, the magnetometer booms are re-stowed and tested on a vibration table, shown in Fig. 13. A low-level ($0.5g$) sinusoidal frequency sweep (sine signature) is first performed from 5–2000 Hz to identify the resonant peaks and their quality factors. Following this, a high-level sweep, or "sine strength" test, is performed up to 50 Hz at $16g$ to verify the mechanism strengths below their natural frequency.

This is followed by a repeat of the sine signature to verify that the frequency response curve has not changed, which would indicate damage. After this, a random vibration test is performed at levels dictated by finite element vibration analysis at the probe carrier and probe level. Finally, the sine signature is performed a third time to again verify the frequency response. All three major axes are tested under sinusoidal and random vibration.

A post-vibration deployment test is performed to test functionality. The booms then stowed and then thermally cycled in vacuum.

The thermal vacuum tests, shown in Fig. 14, consisted of a hot and cold deployment verification in which the booms were first cycled from 75° to −115°C, with a first motion deployment at 50° and −45°C respectfully. The first motion test proves the functionality

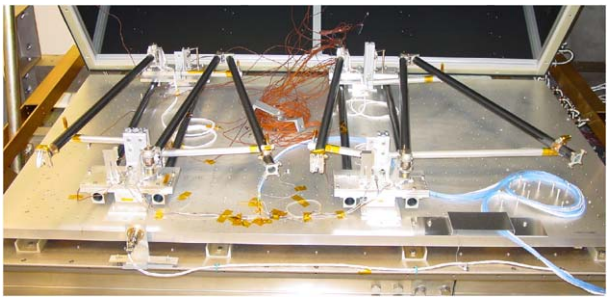

Fig. 14 Thermal vacuum test fixture for magnetometer booms

of the Frangibolt actuator and initial movement in each hinge. The mounting fixtures are designed with the same amount of thermal expansion as the magnetometer booms.

The magnetometer booms underwent three gravity drop tests, in which the boom is mounted to a wall orientated such that gravity would simulate the centripetal acceleration of extended magnetometer boom. The first test is a proof test of the hinges with the kinetic energy from deployments of the spacecraft spinning up to 18 RPM. This is done using scaled mass dummies and allowing the boom to drop from an angle translated from the predicted kinetic energy of a deployment.

The second test tests the repeatability of the final deployed position. The magnetometer boom is deployed from a more moderate angle, and the inclination of the mount is recorded from a mounted 2-axis inclinometer sensor. This test is repeated five times per boom to determine that the alignment/orientation repeatability is better than 0.01°. The third test measures alignment of the magnetometer booms using the inclinometer sensor mounted in two orthogonal positions on the magnetometer mounts and compared the measured angles to reference surfaces on the base hinge. The alignment of the booms are measured, or shimmed if necessary, to be within $\pm 0.1°$ in Z axis from the predicted value. The alignment angles in the other two axes are measured to be within $\pm 0.25°$ of the predicted value. Numerical simulation of the deployment environment is used to verify deployed boom resonance above 0.75 Hz.

3 The Radial Electric Fields Mechanisms

3.1 Overview

The THEMIS Spin Plane Booms (SPB's) deploy the $\pm X$ and $\pm Y$ Electric Field Instrument (EFI) sensors in a radial direction from the spinning spacecraft, as shown in Fig. 1. The deployed boom preamplifiers with attached 3 m sensors are deployed to a tip-to-tip length of 40 m in X and 50 m in Y direction. Each SPB consists of a spool, motor and meter wheel, release mechanism, chassis, Gore composite cable, SPB preamplifier enclosure, and sensor subassembly, as shown in Fig. 15. The four SPB's are mounted to the lower deck of the spacecraft with the snout protruding through a square cutout in the center of each side solar array.

3.1.1 Cable Spool

A spool mechanism safely stores the 21.5 meter sensor cable prior to deployment. The spool electrically isolates the cable from the SPB chassis, allowing the controlled electrical grounding of the outer shield of the cable to the structure to dissipate static charge. The

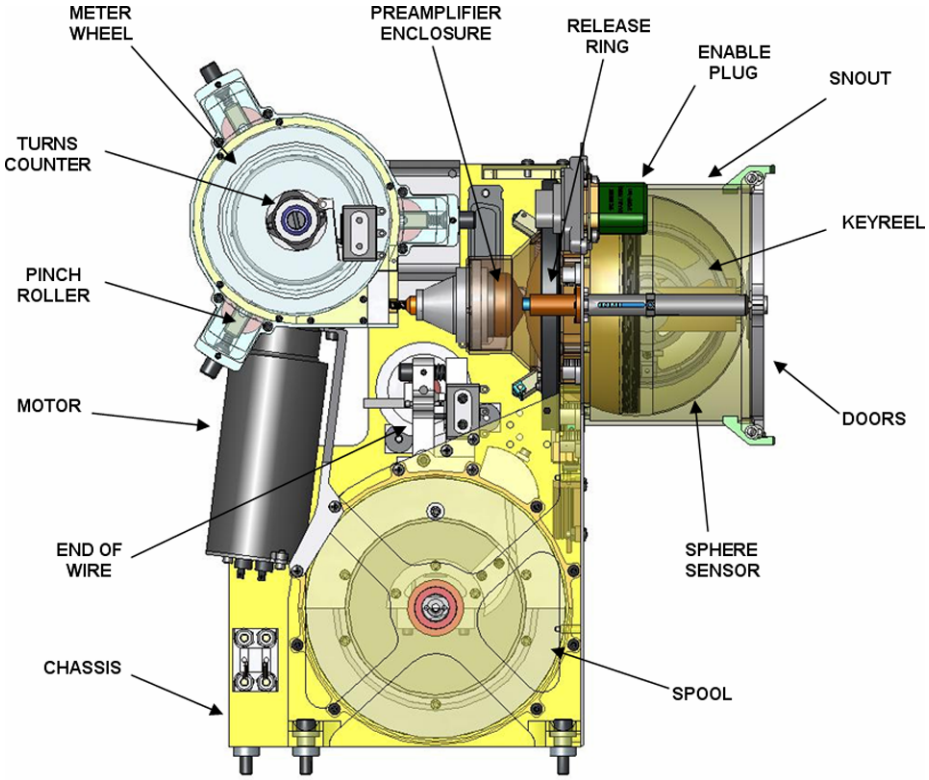

Fig. 15 SPB, transparent view

electrical signals between the rotating spool and the chassis are transferred using slip rings. Each circuit on the slip ring has redundant fingers that improve the electrical noise levels, even though the sensor is not recording accurate E-field measurements during deployment. The spool also anchors the cable and prevents the motor from breaking the cable by strain relieving the cable to a harness cable bracket. An end of wire switch actuates to terminate motor power when an over-tension condition places too much strain on the cable. This over-tension condition can occur when the cable is fully deployed, or if the cable becomes nested and tangled in itself. To ensure the cable does not become nested during launch vibration, a friction brake caliper is adjusted to apply rotational resistance to the spool.

3.1.2 Motor and Meter Wheel

A brushed, DC-powered gear motor deploys the SPB cable and sensor. The motor requires a multi-layer (magnetic attenuating), mu-metal shield to decrease the magnetic dipole created by the motor's permanent magnets. A close-out shield with EMI filters reduces the high frequency electrical noise produced when the motor is in operation, and a diode between the motor terminals helps reduce back-EMF when the motor power is turned off. Bevel gears transmit torque from the motor to the meter wheel through a 90° bend, creating a compact SPB design. The SPB cable lies in a v-shaped grove cut in the vulcanized rubber on the meter wheel outside diameter. Three pinch rollers apply inward radial pressure to the cable to ensure it remains in good contact with the meter wheel, thus creating a capstan force

for the meter wheel to pull the cable from the spool. Cable metering is accomplished by a micro-switch that follows a four-lobed cam, indicating every 4.7 cm deployed. If the end of wire switch fails to prevent an over tension condition in the cable, a shear pin in the meter wheel can also shear to prevent cable damage.

3.1.3 Release Mechanism

While the SPB is stowed, the doors apply sufficient preload to cage the sphere and preamp to avoid damage during launch vibrations. The doors are held closed by two release pins under spring tension, allowing for even loading and compliance. The inboard ends of the pins rests on bearings that are mounted on a titanium release ring. The release ring rotates when voltage is applied to shape memory alloy (SMA) wire. The SMA wires thermally contract, which causes the bearings to roll off the release pins, and release springs force the release pins forward and clear of the doors' travel. An end-of-travel switch is actuated when the release ring is fully rotated, turning off power to the SMA wires to preventing overstress and subsequent loss of wire 'memory' during testing.

3.1.4 Chassis

The chassis consists of a fixed and removable side plate, front plate, support angle, and snout. The structural pieces, with exception of the snout, are made of an aluminum-magnesium alloy and are weight-relief pocketed to decrease overall mass. There are two sheet metal pieces that both support and increase stiffness of the front plate and protect the cable and release ring assembly when thermal blanketing is applied. The chassis is maintained at spacecraft potential through the SPB harness, and is thermally isolated from the spacecraft using Ultem spacers.

3.1.5 Composite Cable

The THEMIS SPB Gore composite cable consists of an inboard connector termination, cable, bead, and outboard preamplifier enclosure termination. Similar configurations are on both ends of the AXB Gore cable discussed in Sect. 4. A section view of the cable is provided in Fig. 16 illustrating how the coax and eight single conductors are held tightly together by a load carrying Kevlar braid. The Kevlar is then wrapped by an aluminized Kapton tape that acts as an electrostatic barrier. The most outer layer is a silver plated copper (SPC) braid that prevents abrasion and wear of the aluminized Kapton. The inboard connector attaches the cable to the spool electrically and serves as an anchor to stress relieve the cable through the Kevlar braid. An epoxy bead is located inboard of the preamplifier enclosure to allow the last 3 meters of cable to be biased at Distal Braid (D-braid) potential, illustrated in Fig. 19. The bead conceals an electrical discontinuity in the outer SPC braid and aluminized Kapton electrostatic barrier, but maintains the axial strength via the Kevlar braid. The outboard preamplifier enclosure termination consists of the cable holder, guard surface of the preamp, sockets and socket holder. The Kevlar strength member is extracted from the cable and anchored to the cable holder to provide strain relief. The coax and single conductors are terminated in sockets that are housed in the socket holder. This forms the inboard end of the preamplifier enclosure.

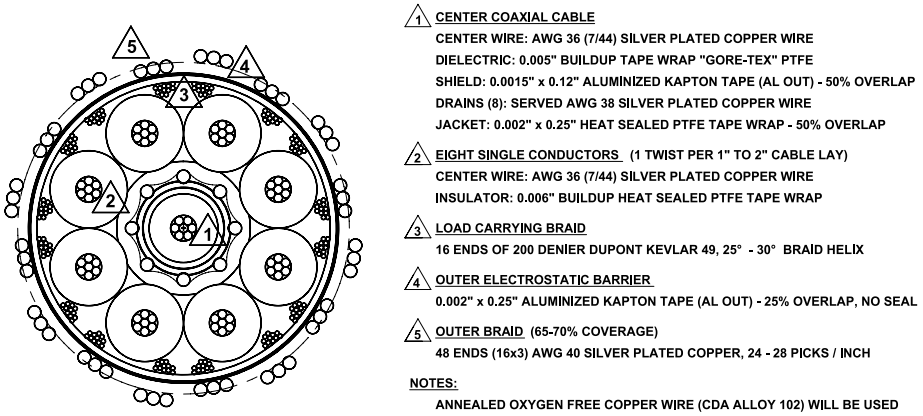

Fig. 16 Gore custom cable construction

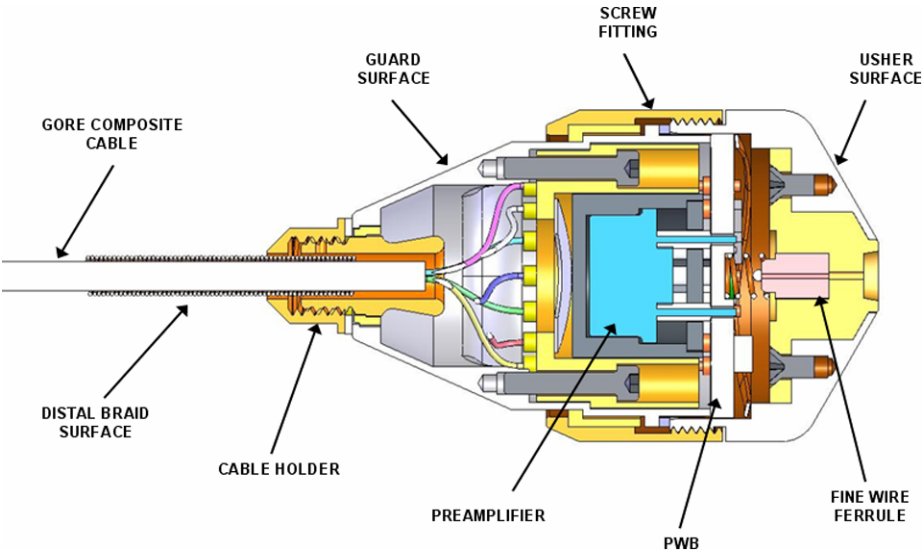

Fig. 17 Preamplifier enclosure, section view

3.1.6 SPB Preamplifier Enclosure

The preamplifier (preamp) enclosure is divided into the inboard cable connector end, the cable preamp printed wire board (PWB), and outboard end as shown in Fig. 17. The inboard preamp end was described in the composite cable section. The PWB contains a few discreet components, an op-amp, and pins that mate with sockets on the inboard end. The outboard end consists of the usher surface and fine wire ferrule. The ferrule is crimped to securely anchor the fine wire that comes from the spherical sensor, and also makes contact with the ferrule spring that is the input to the operational amplifier (op-amp). The preamp is assembled by mating the PWB with the inboard end, mating the outboard end and fine wire ferrule on the PWB, and finally tightening the screw fitting. The usher surface includes the screw

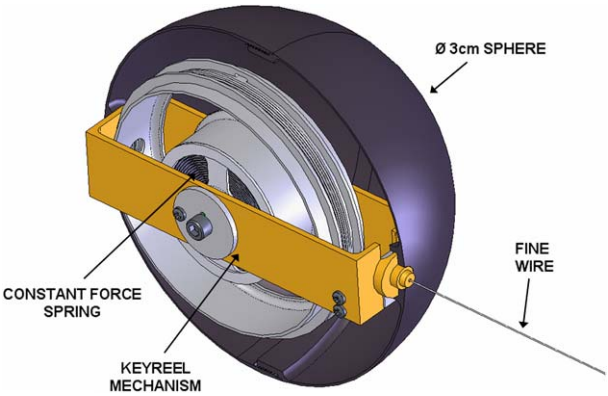

Fig. 18 Sphere sensor, sectioned view

fitting and is electrically isolated from the preamp enclosure guard surface (Guard) and D-braid. Traces on either side of the PWB make contact with the Guard and Usher surfaces and allow each to be biased at a different potential. A tantalum cover and disk enshroud the op-amp for radiation hardening, Careful analysis and design permits the extreme temperature fluctuations that are experienced while deployed well away from the thermally controlled spacecraft. Modular construction of the preamp allows for ease of preamp removal during integration and testing.

3.1.7 Sensor

An ∅8 cm aluminum sphere shell is coupled to a ∅0.25 mm stainless steel fine wire that terminates in the preamp enclosure at the preamp ferrule. Prior to deployment, a constant force spring key-reel mechanism inside the sphere stows the fine wire and prevents the fine wire from nesting and becoming tangled, as shown in Fig. 18. Owing to key-reel spring force, the sensor remains coddled next to the preamp enclosure when the SPB doors are opened. When the sensor and preamp enclosure are deployed to a pre-determined distance from spacecraft and spacecraft spin rate, the centrifugal force overcomes the constant-force key-reel mechanism spring and the sphere deploys the 3 m of fine wire smoothly.

3.1.8 Electric Field Biasing Elements

The best e-field measurements are made when the effects of photo-emissions from the spacecraft and the boom mechanisms are minimized. As discussed in the science section, the potential of various surfaces on the booms need to be controlled separately to accomplish this, illustrated in Fig. 19. The SPB chassis is at spacecraft ground potential, and the proximal Gore cable braid (P-braid) is grounded to the chassis through a 330 kΩ resistor. The D-braid, Guard, and preamp enclosure usher surface (Usher) potentials are biased by circuits through the Gore composite cable from the IDPU. These surfaces help isolate the sensor from the photoemission charge cloud surrounding the spacecraft. The sphere and preamplifier enclosure surfaces have a DAG-213 carbon based coating for a uniform work function and to moderate the on orbit temperatures.

3.1.9 Testing

THEMIS SPB mechanical testing began with a functional test of the sphere sensor key-reel spring mechanism. The sensor assembly was placed on a motorized take-up spool and load

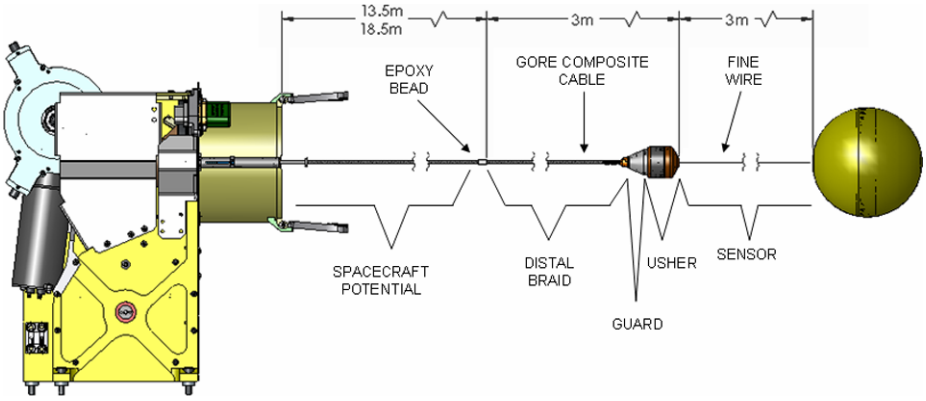

Fig. 19 SPB sensor surfaces

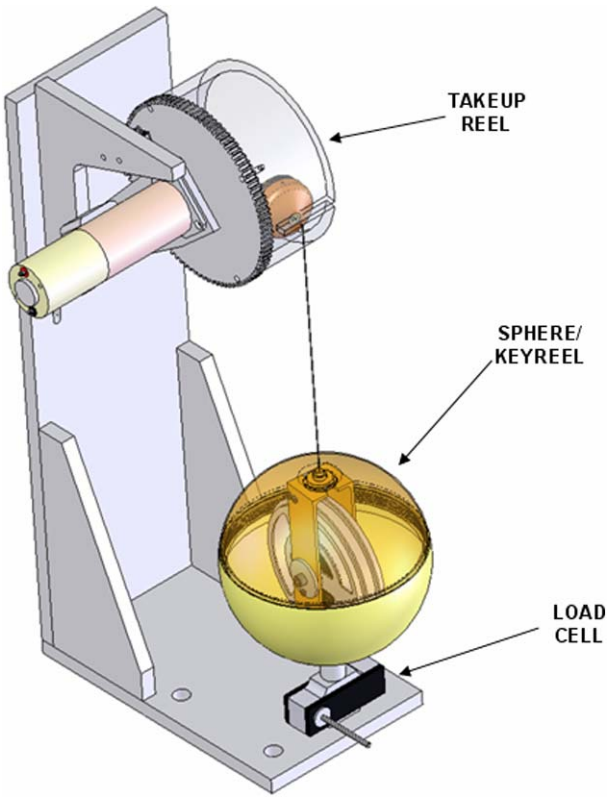

Fig. 20 SPB sphere TVAC GSE for force-deflection characterization

cell apparatus in a thermal vacuum chamber to characterize the force vs. extension of the key-reel spring over extreme operational temperature ranges, illustrated in Fig. 20. This data would indicate at what combinations of spacecraft spin rate and preamp deployed length the sphere sensor would deploy the fine wire.

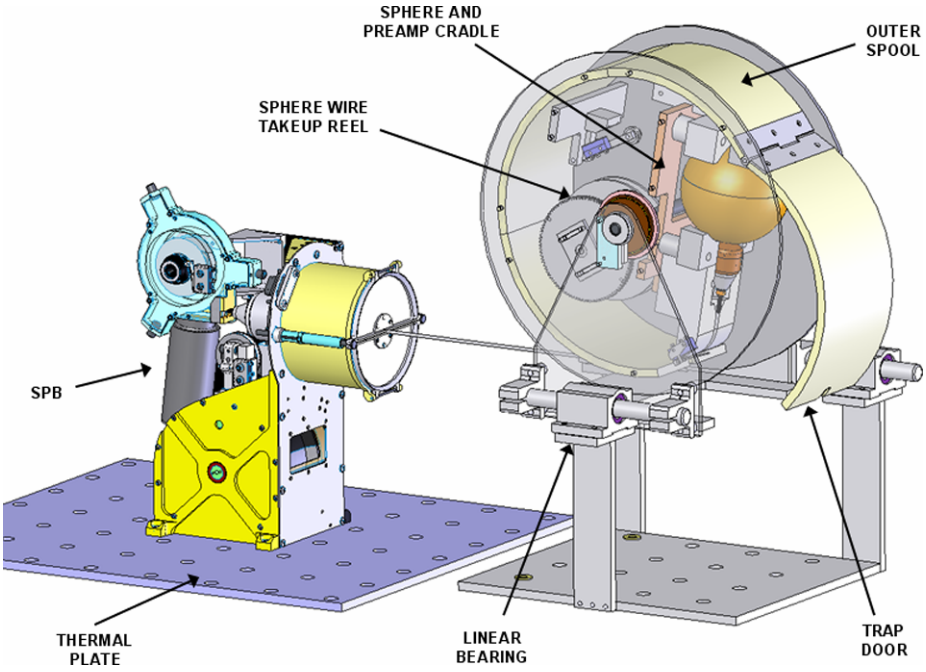

Fig. 21 SPB thermal vacuum test setup, transparent view

Once the sphere sensor was integrated with the SPB cable and preamp, the SPB was stowed and electrical continuity and isolation checks verified that all assemblies were fitted properly and electrical results were as predicted. A functional test deploy and length calibration was performed in the high bay, observing proper door firing, and cable length measurements and meter wheel turns counts were recorded. The SPB was then stowed, and then instrument level sine and random vibration tests were conducted to verify strength design and proper assembly of the SPB.

After a post-vibration electrical continuity and isolation test, the SPB was then placed in a thermal vacuum (TVAC) chamber with a sphere, cable, and preamp take-up device to conduct an end-to-end deployment of the SPB at extreme operational temperatures of -25 to $+55$°C, as illustrated in Figs. 20 and 21. Nominal current and release time for door firing, SPB motor current, preamp quiescent current, deploy time, and meter wheel turns counts were recorded. The full length of fine wire and Gore cable was deployed to ensure the end of wire switch operated properly to prevent cable damage.

Upon completion of TVAC testing, the SPB was stowed, electrical continuity and isolation was performed, and finally delivered for integration and further instrument suite level testing.

4 The Axial Electric Fields Mechanisms

4.1 Axial Boom Science Configuration

Deployable rigid booms are provided to hold the whip sensors on the spacecraft spin axis to make the Z-axis E-field measurement. The two boom deployment mechanisms are mounted

in a tube that forms the central structural element in the THEMIS bus. This tube also serves as the antenna mount. The deployed boom elements are each 2.44 m long, topped with a preamplifier module and a 0.75 m whip sensor, forming a 6.4 tip-to-tip sensor array. The main elements are grounded to the bus to hold them at spacecraft potential. A nine conductor cable runs inside each boom element to the preamp, and the whip sensor is the preamp input. The outer surface of the preamp module is divided into Guard and Usher surfaces that are each electrically driven, as in the Spin Plane Booms.

4.2 Axial Boom Design

Each axial boom consists of a Stacer boom element, a deployment assist device (DAD) with roller nozzles, a preamp, a Stacer whip sensor, and a cable and bobbin. The boom is caged for launch by a Frangibolt shape-memory alloy device. The two axial booms are mounted diametrically opposed in a carbon fiber tube assembly.

4.3 Stacers

The extendible portions of the spin axis booms and whip sensors are Stacers, shown in Fig. 22. The main boom Stacer is a tubular spring element fabricated from a 0.10 mm thick $\times$ 127 mm wide strip of Elgiloy (a non-magnetic super-alloy). It is helically formed such that when released, it forms a slightly tapered, stiff, hollow tube 1.98 m long. The main Stacer stows into a 127 mm long by 50 mm diameter canister. As it is stowed, the coils are manually

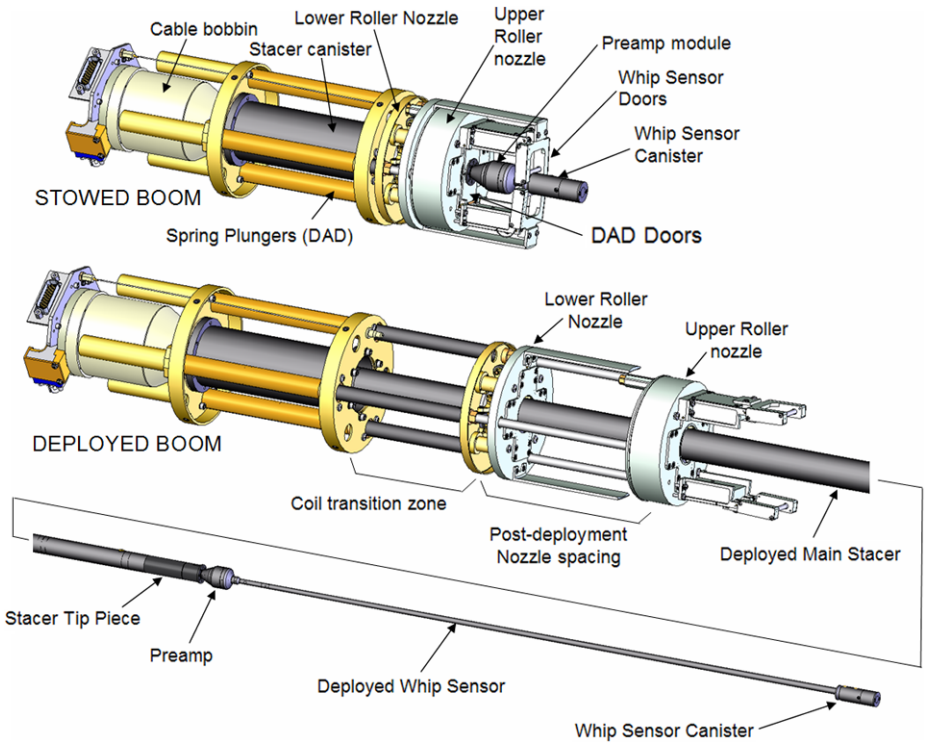

Fig. 22 Axial boom configuration

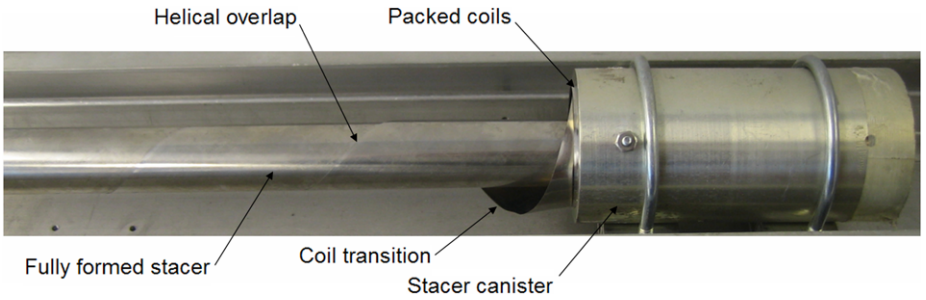

Fig. 23 Stacer deployment

packed out against the canister I.D., increasing the coil diameter. As the Stacer deploys, the coils curl inward and protrude axially, cinching around first the tip piece, and subsequently around the previously deployed coils illustrated by Fig. 23. This change in diameter during the unfurling provides the strain energy that generates the deployment push force. Thus, the Stacer deployment is self-powered. The tip piece is slightly larger than the strip free-coil diameter, so that the coils grab tightly. This generates enough friction between coils that they do not easily slip on one another, giving the Stacer has a bending stiffness similar to a tube with comparable wall thickness for small deflections. The stacking of subsequent coils causes a buildup in deployed diameter, leading to the gradual taper from the 18 mm diameter tip the 23 mm diameter base. This taper gives better bending stiffness and mass properties than constant diameter booms. The sensor Stacer is a smaller version with a strip thickness of 0.05 mm, a length of 0.75 m, and base and tip diameters of 7.9 mm and 6.4 mm. The Stacer elements mass is 270 g and 7 g for the mains and whips respectively.

A primary advantage of Stacers, as compared to other types of long rigid booms such as Stem booms, is the Stacer's thermal symmetry. The poor thermal conductivity between the two axial strips forming a Stem boom can produce significant asymmetries in its thermal bending, which has been known to cause thermal pumping on spacecraft such as Ulysses. The helical overlap of the single Stacer strip, by contrast, provides a helically symmetric path for heat flow from the sun-lit to shadowed sides of the Stacer. This leads to a small, but uniform deflection 90° from the sun line that does not excite spacecraft wobble.

4.4 Boom DAD and Roller Nozzles

Two roller nozzles are used to give the main Stacer the required cantilever stiffness. Because the Stacer coils are not well supported in the transition zone between the canister and the fully formed Stacer, it has no inherent stiffness at its root. The necessary support to make it a stiff cantilever is provided by two roller nozzle assemblies spaced approximately 130 mm apart when deployed. These are positioned beyond the Stacer canister by means of a telescoping two-stage Deployment Assist Device (DAD), included in Fig. 22. This design has a compact stowed geometry while providing the necessary separation between the nozzles to give a rigid pinned-pinned base attachment.

The expanding roller nozzle design, illustrated in Figs. 24 and 25, provides play-free positioning despite the changing boom diameter during deployment, while also minimizing friction. The four ball bearing rollers are held on pivoted rocker arms attached to a common cover that is pulled by spring cartridges towards the base plate. Idlers on each rocker arm roll on the base plate, rotating the rollers inwards in a pinching motion, providing play-free

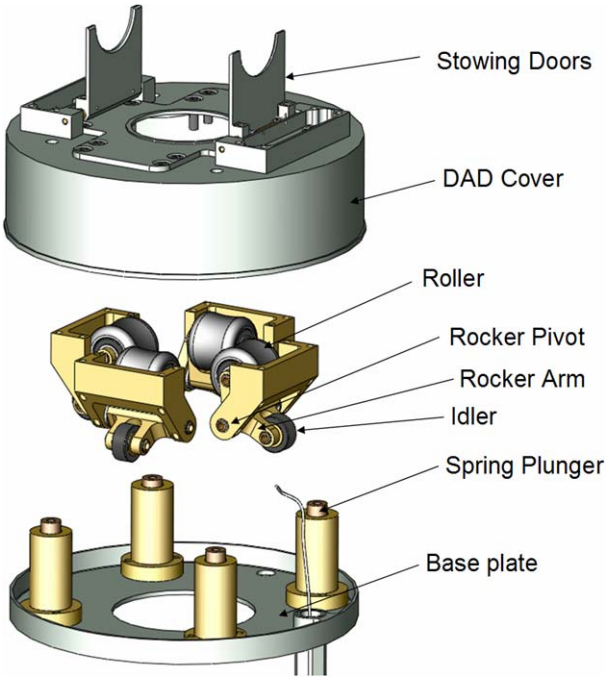

Fig. 24 Roller nozzle components

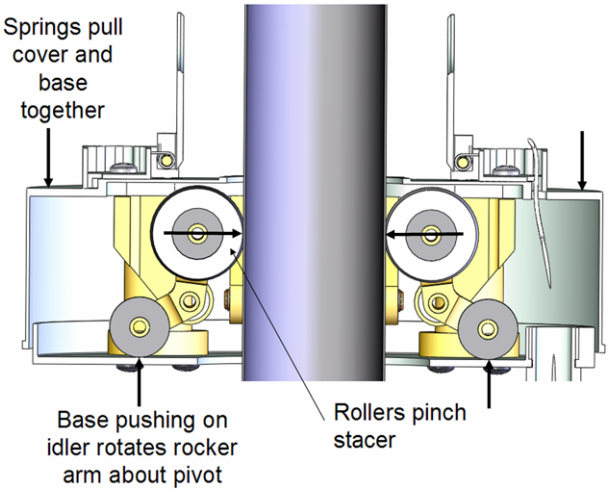

Fig. 25 Roller nozzle operation

lateral constraint and centering for the Stacer while allowing it to roll outward freely during deployment.

The roller nozzles are held together and against the canister for launch by trap doors that catch an edge on the Stacer tip piece, shown in Fig. 26. The nozzles are pushed beyond the coil transition zone and apart by telescoping spring loaded plungers when the boom is released. A second outer set of doors cages the small whip sensor Stacer. The plungers also provide an initial kick force to help the cinching of the first coil on the tip piece, ensuring correct formation of subsequent coils. After the Frangibolt initiated release, the DAD

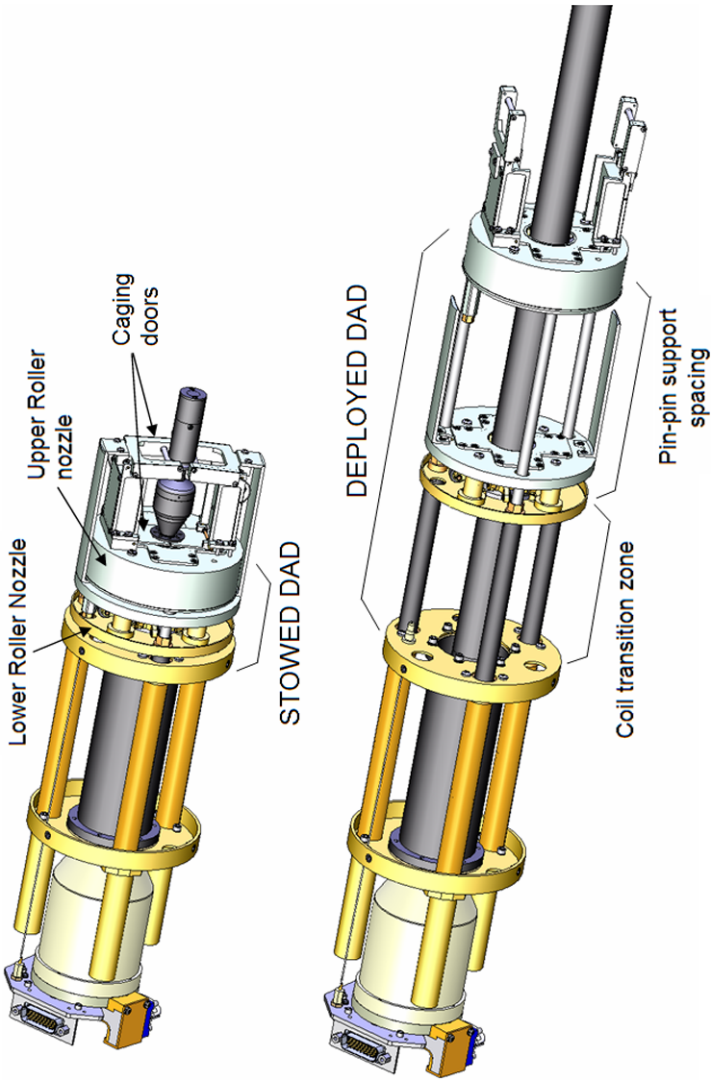

Fig. 26 DAD deployment

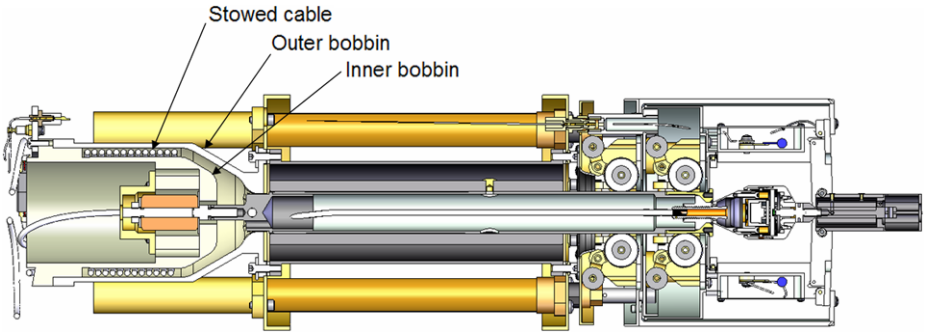

Fig. 27 Cable bobbin

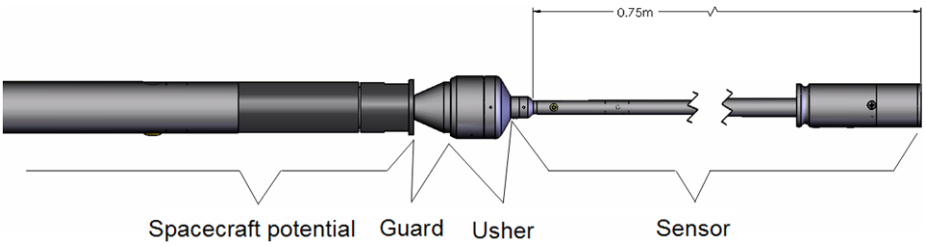

Fig. 28 Sensor surfaces

plunger pushes the tip piece to beyond the coil forming zone of the Stacer, and the trap doors are pushed open by the deploying boom. Once the deployment is initiated, the Stacer makes contact with the rollers and these allow only axial motion.

The final length of the main Stacer is controlled by a cable that is stowed in a bobbin at the aft end of the canister illustrated in Fig. 27. During deployment, this cable pulls off of the bobbin, and strops the deployment at the desired length. This cable, of the same construction as for the Spin Plane booms, provides the necessary conductors to the preamp, as well as a Kevlar layer that absorbs the end-of-stroke deployment energy.

4.5 Electric Field Biasing Elements

The best E field measurements are made when the effects of photo-emissions from the spacecraft and the boom mechanisms can be minimized. As discussed in the science section, the potential of various surfaces on the booms need to be controlled separately to accomplish this. The main Stacer and its tip piece are grounded to the spacecraft through a 1 MΩ resistor. The guard and usher potentials are controlled through lines running back to the instrument IDPU, shown in Fig. 28. These surfaces can be biased to help isolate the sensor from the charge cloud surrounding the spacecraft. The whip and its canister form the sensor surface and are the input to the preamp. All external surfaces are conductive to minimize charging, and are coated with DAG 213 carbon based paint for a uniform work function and to moderate temperatures. A UCB designed electrical connector between the preamp and Stacer tip piece allowed swapping of the sensors without disturbing the stowed boom.

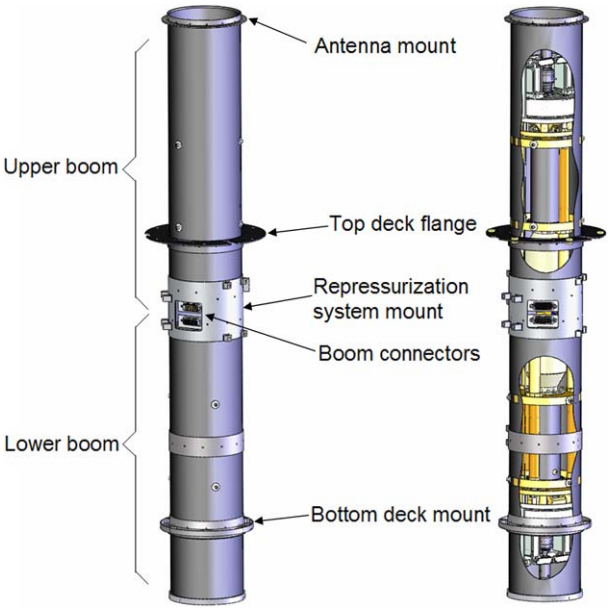

Fig. 29 Boom mounting tube

4.6 Boom Mounting Tube

The axial boom mechanisms are held in the THEMIS spacecraft by a mounting tube assembly. This tube holds the booms coaxial with the spacecraft Z axis. It also serves as a structural member in the spacecraft bus, supporting the top deck at its center and providing needed supports for the probe RCS re-pressurization system and antenna. The tube is 0.86 m long, and extends 0.33 m above the spacecraft top deck, supporting the S-band antenna well away from spacecraft.

The pair of boom assemblies is mounted in a 100 mm diameter thin wall graphite-epoxy tube that is manufactured by the UCB Composites Lab. The tube consists of 5 layers of a Fiberite 0.13 mm thick prepreg woven graphite fiber material. The inner, middle and outer layers were laid at 0°–90°–0° and the layers between were set to ±45° to the tube axis. Titanium, aluminum, and carbon fiber flanges are mounted to the outside of the tube to provide mounting points for the flanges to bolt the boom to the spacecraft top and bottom decks, the antenna, as well as to support the re-pressurization system. Because the mounts are structural components of the spacecraft, these were completed early in the program so that they could be shipped to the spacecraft contractor for incorporation onto the spacecraft structure for the bus structural testing.

4.7 Axial Boom Testing

In-air testing of the axial booms was performed in two ways. Initially the booms were deployed upward vertically to yield a non gravity-biased concentricity measurement. The unit was mounted coaxially on a turn table base, and after deployment, the unit was rotated to measure the total tip run-out. Each boom was then deployed with the tip piece attached to a low friction trolley on a horizontal track. This horizontal deployment gives a more accurate length measurement with the absence of gravity in the deployment direction. For environmental testing, the individual boom units were subjected to 3 axis sine and random vibration,

and then 12 cycles of thermal vacuum with hot and cold deployments. The horizontal deployment track was also used here. After hot and cold soaks at −60°C and +75°C, each boom was deployed down the trolley in a long vacuum tight tube attached to the chamber. One boom was deployed hot (+40°C), the other cold (−35°C). A final verification deployment was performed after inspection, The final step was inspection and stowing for launch. Deployed boom straightness was found to be within 3–19 mm at its 3.2 m length, and the measured lateral resonance was 1.5–1.6 Hz.

5 On-Orbit Performance

The five THEMIS micro-satellites were launched on a common carrier by a Delta II, 7925 heavy, on February 17, 2007. The probe fuel capacity would only accommodate two years of science operations, with the prime science season in February. For these reasons, stage I (2/15/07–9/15/07) of the mission was a coast phase, where the probes were kept in their post launch orbits. The EFI booms on two of the probes were deployed for early science and for mission diagnostics. The booms on the remaining probes remained stowed, so that they could be maneuvered to higher orbits with better fuel efficiency. All probe magnetometer booms were deployed shortly after launch. Stage II (9/15/07–12/15/07) of the mission was the orbit placement period. The probes were maneuvered to their assigned 0.8, 1, 2, and 4 day orbits. Following this orbit placement, EFI booms on the remaining three probes were deployed. In all, 40 boom mechanisms were deployed on the five probes with no failures or anomalies. Careful planning by the Berkeley Mission Operations team resulted in no improper maneuvers on orbit. The probe dynamic behavior, during RCS maneuvers and boom deployments was as predicted and tested. Post maneuver settling times were near real time, when compared to next command formulation and execution. Mission stage III prime science began on 12/15/07 with all five probes fully operational.

6 Summary

The THEMIS boom mechanism designs have evolved over a period of thirty years, from a long series of successful satellite instruments flown on S3-3, ISEE, Viking, Freja, CRRES, Polar, FAST and Cluster 1 & 2. The Themis mission was a unique opportunity to advance the state of the art of the three boom systems it employed. It was predicated as a higher risk mission with a short development and fabrication cycle. The five probes are achieving their primary science objectives, and by doing so, provided an engineering development history for future missions to call upon.

Acknowledgements The authors wish to thank the Explorers Office at NASA Goddard Space Flight Center for funding this mission under contract NAS5-02099. Dr. Vassilis Angelopoulos, University of California Berkeley was the energetic and motivated THEMIS Principal Investigator. Frank Snow was the GSFC Mission Manager and Peter Harvey was the UCB Project Manager. Both managers were enthusiastically motivating and played a critical role in achieving our first proposed launch date.

References

V. Angelopoulos, The Themis mission. Space Sci. Rev. (2008, this issue). doi:10.1007/s11214-008-9336-1

D.M. Auslander, An object-oriented approach to basic mechanics, in *Proceedings of the ASME International Mechanical Engineering Conference & Exposition*, Orlando, FL, Nov. 2000, pp. 771–778

F.T. Dodge, *The New "Dynamic Behavior of Liquids in Moving Containers"* (Southwest Research Institute, San Antonio, 2000)
S.T. Lai, K.H. Bhavnani, Dynamics of satellite wire boom systems, AFCRL-TR-75-0220, 1975
L. Meirovitch, R.E. Calico, The stability of motion of satellites with flexible appendages. NASA CR-1978, 1972